Hindawi
Journal of Nanomaterials
Volume 2019, Article ID 5384132, 13 pages
https://doi.org/10.1155/2019/5384132

Research Article

Highly Crystalline WO_3 Nanoparticles Are Nontoxic to Stem Cells and Cancer Cells

B. Han,[1] A. L. Popov,[2] T. O. Shekunova,[3,4] D. A. Kozlov,[3] O. S. Ivanova,[4] A. A. Rumyantsev,[4] A. B. Shcherbakov,[5] N. R. Popova,[2] A. E. Baranchikov,[3,4] and V. K. Ivanov[4,6]

[1]*Jiangsu University of Technology, Changzhou 213001, China*
[2]*Institute of Theoretical and Experimental Biophysics, Russian Academy of Sciences, Pushchino 142290, Russia*
[3]*Lomonosov Moscow State University, Moscow 119991, Russia*
[4]*Kurnakov Institute of General and Inorganic Chemistry of the Russian Academy of Sciences, Moscow 119991, Russia*
[5]*Zabolotny Institute of Microbiology and Virology, National Academy of Sciences of Ukraine, Kyiv D0368, Ukraine*
[6]*National Research Tomsk State University, Tomsk 634050, Russia*

Correspondence should be addressed to V. K. Ivanov; van@igic.ras.ru

Received 26 September 2018; Accepted 10 February 2019; Published 28 April 2019

Academic Editor: Elisabetta Comini

Tungsten oxide sol, containing highly crystalline nanoparticles of orthorhombic WO_3 and having good sedimentation stability, was synthesized using a facile, ultrasonic-assisted technique. An additional steric stabilizer, dextran, was proposed to enhance the stability of WO_3 nanoparticles in biological media and to reduce their *in vivo* toxicity. The cytotoxicity of dextran-stabilized and nonstabilized WO_3 sols was studied *in vitro* using dental pulp stem (DPS) cell lines and breast cancer (MCF-7) cell lines. Both tungsten oxide sols demonstrated low cytotoxicity and low genotoxicity for both stem cells and malignant cells and only slightly reduced their metabolic activity in the concentration range studied (from 0.2 to 200 μg/ml). The data obtained support possible theranostic applications of tungsten oxide colloidal solutions.

1. Introduction

Tungsten trioxide (or tungsten(VI) oxide. WO_3 is a semiconductor material with a bandgap width of 2.5–2.8 eV that corresponds to the visible spectrum range. WO_3 nanoparticles and nanocrystalline thin films have a wide range of applications in microelectronics and optoelectronics [1], in smart windows [2, 3], in dye-sensitized solar cell engineering [4], in gas-sensing devices [5–7], in quantum dot-based light-emitting diodes [8], in catalysis [9, 10], in photocatalysis [10–12], and in photoelectrocatalysis [13], including water splitting [14–16], wastewater purification [17], and disinfection [18–22].

Recently, tungsten oxide has attracted a great deal of attention due to its promising biomedical applications [23–25]. WO_3 nanoparticles strongly enhance the visibility of tissue structures in X-ray-based imaging techniques, namely, computed tomography (CT). The X-ray absorption coefficient of tungsten (4.438 cm^2/kg at 100 keV) is much higher than that of convenient CT contrast agent iodine (1.94 cm^2/kg at 100 keV) [26]. Tungsten oxide nanoparticles possessing photocatalytic properties [22, 27, 28] have been applied in photothermal [22, 26, 29, 30] and photodynamic [22, 30–32] therapies. Tungsten oxide nanoparticles act as a radiation dose-intensifying agent during radiation therapy [32] and can be used as a theranostic agent for simultaneous tumour CT imaging and therapy (trimodal action: photothermal, photodynamic, and radiation [32]). The safety and hazard data on WO_3 is available at PubChem [33].

In cancer theranostic applications, photoactive semiconductor nanoparticles should possess two equally important properties: minimum toxicity in the dark (for normal cells)

and maximum activity upon irradiation (for tumour cells). Both of these requirements can partially be satisfied by means of varying the particles' surface state and habitus during synthesis.

The habitus of tungsten oxide nanostructures can easily be adjusted to the application requirements. In this way, 0D (dots), 1D (rods, whiskers, and fibres), 2D (plates, films), or 3D (large particles, blocks) WO_3 materials can be synthesized. Various types of nanostructured tungsten oxide have been reported, from simple, spherical nanoparticles [34] to WO_3-based aerogel networks [35], quantum dots [36–39], nanostructured films [40] (including nanoplate films [41], nanorod films [42], honeycomb-structured films [43], and mesoporous films [44]), nanobelts [45], nanofibres [46], nanowires [30, 46, 47], bundle-like nanowires [30, 48], nanonetworks [49], hollow spheres [50], macroporous spheres [51], wedge-like architectures [52], nanorods [53, 54], nanocuboids [34], square nanoplates [55], nanosheets [56], nanoleaves [57], and urchin-like [30, 58], flower-like [59–61], and tree-like nanostructures [62, 63], etc.

Several sophisticated approaches have been developed for the synthesis of WO_3 nanostructures using vapour-, liquid-, and solid-phase (both "wet" and "dry") methods [19]. The vapour-phase route can be realized *via* laser ablation [64], electron beam irradiation [65], ion bombardment [66], or heat treatment [67] of tungsten-based materials; these techniques are used primarily for the production of nanostructured films and include such processes as sputtering [68] and thermal evaporation (including hot-wire [69, 70] and arc discharge vaporization [71] and spray pyrolysis [72–74]). The key liquid-phase approaches for the synthesis of WO_3 nanoparticles include precipitation with acids [75], hydro- or solvothermal treatment (using aqueous [76–78], nonaqueous [20, 79], or mixed [80] solvents), sol-gel processing (both in aqueous [81, 82] and in nonaqueous [83] systems), reverse microemulsion-mediated routes [84–87], and soft [21, 88] and hard [89] templating (including electrodeposition [90]). Solid-phase methods are based mainly on two approaches: tribochemical [91] and thermal [92] decompositions; the latter allows the production of a pure, surfactant-free, well-crystallized material without harmful impurities. For example, ammonium meta- and paratungstate are readily decomposed under heating, to form tungsten trioxide [93–102].

It is a well-known fact that the photoactive properties of WO_3 nanoparticles depend strongly on the crystallinity of this material: the increase in the crystallite size enhances the photodecomposition rate of organic materials [103] and, similarly, the photocytotoxicity of the nanoparticles [28]. On the other hand, an increase in crystallinity and a decrease in the hydration degree of the tungsten oxide surface (e.g., upon solvent-free synthesis of WO_3 nanoparticles) should be accompanied by a decrease in their solubility and toxicity, since the cytotoxicity of WO_3 nanoparticles (including genotoxic effects such as DNA damage and micronuclei) is supposedly caused by free tungsten ions [104], which could induce oxidative stress and inflammation. In this paper, we have tried to clarify these controversial issues by analyzing the cytotoxicity of the original surfactant-free aqueous WO_3 sol, prepared by solid-state thermal decomposition of ammonium paratungstate, followed by ultrasonic dispersion of the resulting product in water. This sol contains highly crystalline orthorhombic tungsten oxide nanoparticles, which are expected to have low ionic solubility and toxicity and high photoactivity under irradiation. To increase the *in vivo* stability of the sol, it was additionally modified by the nontoxic stabilizer, dextran. Thus, the paper was aimed at the comparative study of the dark cytotoxicity and metabolic activity of normal stem cells and malignant cells in the presence of stabilized and nonstabilized sols of highly crystalline WO_3. For the toxicity studies, we have chosen highly crystalline single-phase WO_3 to exclude any other factors which may affect the toxicity of nanoparticles.

2. Materials and Methods

2.1. WO_3 Nanoparticles' Synthesis and Characterization. WO_3 aqueous sols were prepared using a recently reported protocol [102]. Briefly, 3 g of ammonium paratungstate (high-purity grade) powder was introduced, for 10 min, into a muffle furnace preheated to 600°C, in air. Thus, the obtained WO_3 powder was quenched in air, cooled and mixed with 200 mL of distilled water, and ultrasonicated in an ultrasonic bath for 6 hours to obtain a whitish yellow turbid sol. The sol was allowed to settle for an additional 3 hours and was divided into 2 portions. To one of the portions, dextran powder (high-purity grade, Sigma #31388, 0.162 g) was added and allowed to dissolve under stirring. The concentration of the stock sols as estimated using gravimetric analysis was 2 g/L. Powder X-ray diffraction (XRD) analysis was carried out using a Bruker D8 Advance diffractometer (CuKα-radiation). The scanning electron microscopy (SEM) images were obtained on a Carl Zeiss NVision 40 electron microscope at an accelerating voltage of 1 kV. Before XRD and SEM measurements, the sols were dried in air at 50°C overnight. Time-resolved dynamic light scattering (DLS) measurements of WO_3 suspensions' aggregation behaviour were performed using a Photocor Complex analyzer equipped with a helium-neon laser ($\lambda_{em} = 632.8$ nm). All DLS measurements were conducted at a scattering angle of 90°.

2.2. Cell Culture. Two types of cells were used in the experiments: dental pulp stem (DPS) cells and the breast cancer cell line MCF-7. It should be noted that recent studies have shown a great deal of interest in stem cells for the delivery of antitumour drugs [105–108]. DPS cells were isolated from the third molar germ extracted for orthodontic indications from a healthy, 16-year-old patient. The MCF-7 breast cancer cell line was obtained from the cell bank of the Institute of Cell Biophysics of the Russian Academy of Sciences. The cells were extracted with DMEM (PanEko, Russia) containing 200 U/mL penicillin and 200 μg/mL streptomycin (Life Technologies, USA), with a syringe inserted into the dental apex and further treated with 0.25% trypsin and 0.02% EDTA (Life Technologies, USA) for 30 min at 37°C. The isolated cells were centrifuged for 2 min at 1500 rpm and resuspended to a single cell state in a culture medium consisting of DMEM/F-12 (1 : 1; Life Technologies), with the addition of

10% fetal calf serum (FCS). The obtained solution was transferred into 25 mL vials and cultured in a 5% CO_2 atmosphere at 37°C with the addition of 10% FCS (HyClone), 100 U/mL penicillin/streptomycin, and 2 mM L-glutamine in DMEM (PanEko, Russia). When the subconfluent cell state was achieved, the cultured cells were treated with 0.25% EDTA-trypsin solution and passaged in 75 cm^2 vials in a ratio of 1 : 3. Cells were cultured in DMEM/F-12 (PanEko, Russia), with the addition of 10% FCS, 100 U/mL penicillin/streptomycin, and 2 mM L-glutamine.

2.3. MTT Assay. The determination of mitochondrial and cytoplasmic dehydrogenases activity in living cells was carried out using a MTT assay based on the reduction of the colourless tetrazolium salt (3-[4,5-dimethylthiazol-2-yl]-2,5-diphenyltetrazolium bromide (MTT)). After 24 hours of cell incubation with different concentrations of WO_3 nanoparticles, 0.5 mg/mL of the MTT reagent was introduced into the wells by replacing the culture media, followed by a standard MTT assay.

2.4. Live/Dead Assay. Assessment of the viability of the cells cultured in the presence of WO_3 nanoparticles was performed on a Carl Zeiss Axiovert 200 microscope. An L-7007 LIVE/DEAD BacLight Bacterial Viability Kit (Invitrogen) was used for the assay, which included a SYTO 9 fluorescent dye (absorption 420 nm, emission 580 nm) and a propidium iodide (PI) dye (absorption 488 nm, emission 640 nm). The dyes were added to the medium (1 μg/mL), and the plate was placed in a CO_2 incubator for 15 min. Microphotographs were taken after washing the cells with a phosphate-buffered saline.

2.5. Mitochondrial Potential. Mitochondrial membrane potential (MMP) was determined by JC-1 dye, using fluorescence microscopy according to the standard procedure [109]. JC-1 accumulates in the mitochondrial membrane in a potential-dependent manner. The high potential of the inner mitochondrial membrane facilitates the formation of the dye aggregates (J-aggregates) with both excitation and emission shifted towards red light (530 nm/590 nm) when compared with that for JC-1 monomers (485 nm/538 nm) [109]. Cells were seeded into 96-well tissue culture plates (Greiner) at a density of $5{\cdot}10^4$ cells/well in 100 μL culture medium and cultured in a CO_2 incubator at 37°C for 24, 48, and 72 hours. The cells were preincubated with 5 μM JC-1 in the HBSS in a CO_2 incubator at 37°C for 30 min. Next, the cells were washed twice using HBSS and analyzed using a 200M Zeiss inverted fluorescence microscope (Zeiss, Germany) at 200x magnification. Results are shown as a ratio of fluorescence, measured at 530 nm/590 nm (aggregates) to that measured at 485 nm/538 nm (monomers).

2.6. Fluorescent Staining of Cell Nuclei with Hoechst 33342 Dye. Cells were cultured in 96-well plates, as described above. After 24, 48, and 72 hours of culturing with WO_3 nanoparticles, the cells were washed with HBSS, prior to 20 min staining with Hoechst 33342 (1 mg/mL). Images of stained cells were captured by fluorescence microscopy, and the percentage of apoptosis was calculated by counting (there were >600 cells per group).

2.7. Statistical Analysis. The experiments were carried out in 3-4 replicates, and analytical determinations for each sample were performed in duplicate. The results of the experiments were compared with the control experiment. Methods of variation statistics were applied to estimate the reliability of the results. To assess the statistical significance, the Mann-Whitney U test was used ($p \leq 0.05$). The obtained data were processed using Microsoft Excel 2007 software.

3. Results and Discussion

WO_3 sols, both nonstabilized and stabilized by dextran, demonstrated very good sedimentation stability. After 7 days of storage, the volume fraction of clear liquor did not exceed 7% (Table S1, Supplementary Information). According to X-ray powder diffraction data (Figure 1(a)), the sols obtained were composed of highly crystalline orthorhombic tungsten trioxide (β-WO_3) with a particle size of 65 ± 2 nm, as calculated using a full-profile analysis of X-ray diffraction patterns. SEM images (Figure 1(b)) were in good agreement with the XRD data and showed that ultrasonication resulted in complete disintegration of WO_3 aggregates with the formation of free-standing particles.

The results of the DLS study show that the hydrodynamic diameter of nonstabilized particles was about 54 nm (radius 27 nm); for dextran-stabilized nanoparticles, this value was doubled (Figure 2).

For the cytotoxicity analysis of WO_3 nanoparticles, two types of human cell cultures were selected: normal (stem), isolated from the pulp of a healthy donor's tooth, and transformed, isolated from a breast tumour. This choice was made taking into account their different metabolic activity, morphology, and proliferative activity. From the results of the MTT test, it is clearly seen that MCF-7 cells (Figure 3(a)) proliferated much faster than DPS cells (Figure 3(b)). The analysis of the metabolic activity of MCF-7 and DPS cells using the MTT test after incubation with WO_3 nanoparticles, at all the concentrations tested (0.2–200 μg/mL), did not reveal any significant difference with the control group for both types of cell culture. The differential analysis of the ratio of live/dead cells (Figure 4) after incubation with WO_3 nanoparticles also did not reveal significant differences with the control group. Morphological features of DPS cells after incubation with WO_3 nanoparticles remained unchanged; cells retained the characteristics of fibroblast-like cell cultures, including effective adhesion, spreading, and migration by the leading edge scheme. MCF-7 cells also retained their original morphology and activity after incubation with WO_3 nanoparticles, which additionally confirmed the absence of a toxic effect.

Oxidative stress is the major mechanism of the cytotoxic action for the metal-based nanomaterials [110]. The development of oxidative stress can be associated with a disturbance in the mitochondrial metabolism, which leads to an increase of the intracellular ROS level [111]. It is also well known that nanocrystalline tungsten is capable of generating ROS in

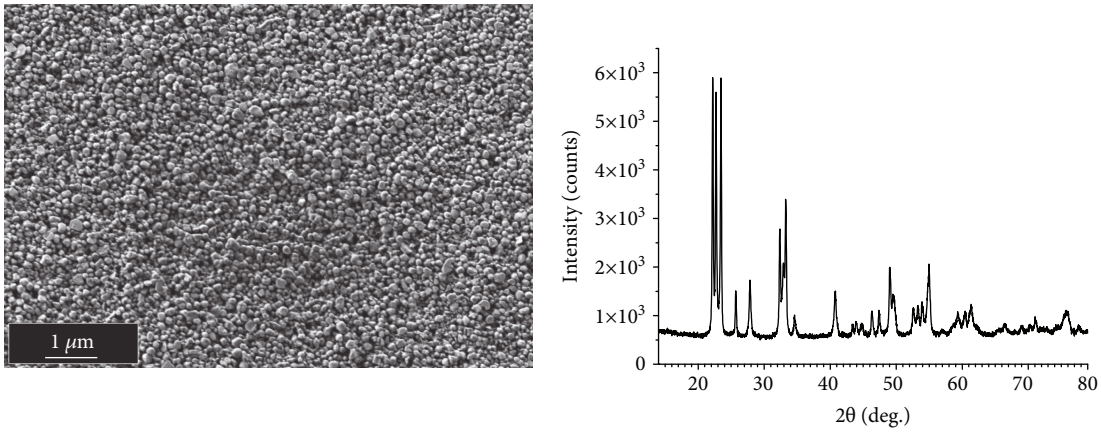

(a) (b)

Figure 1: The SEM image (a) and X-ray diffraction pattern (b) of WO_3 nanoparticles.

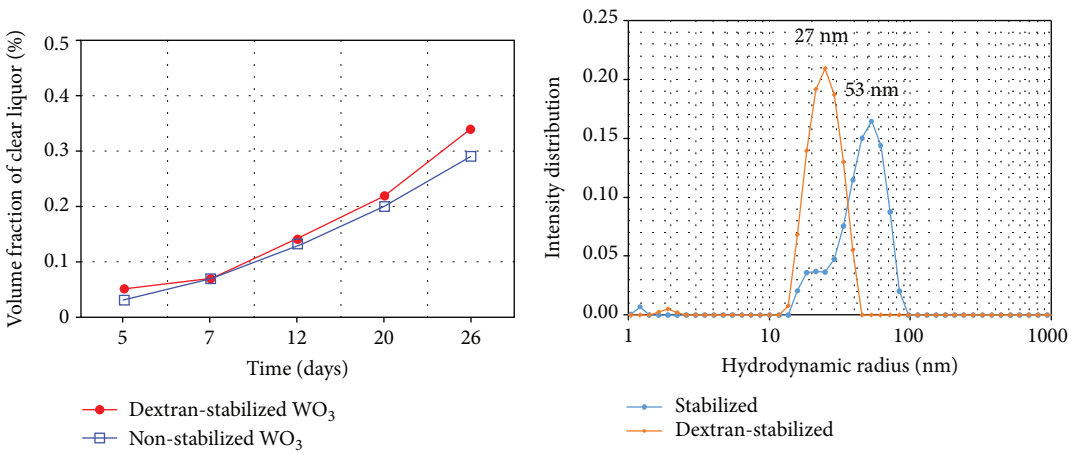

(a) (b)

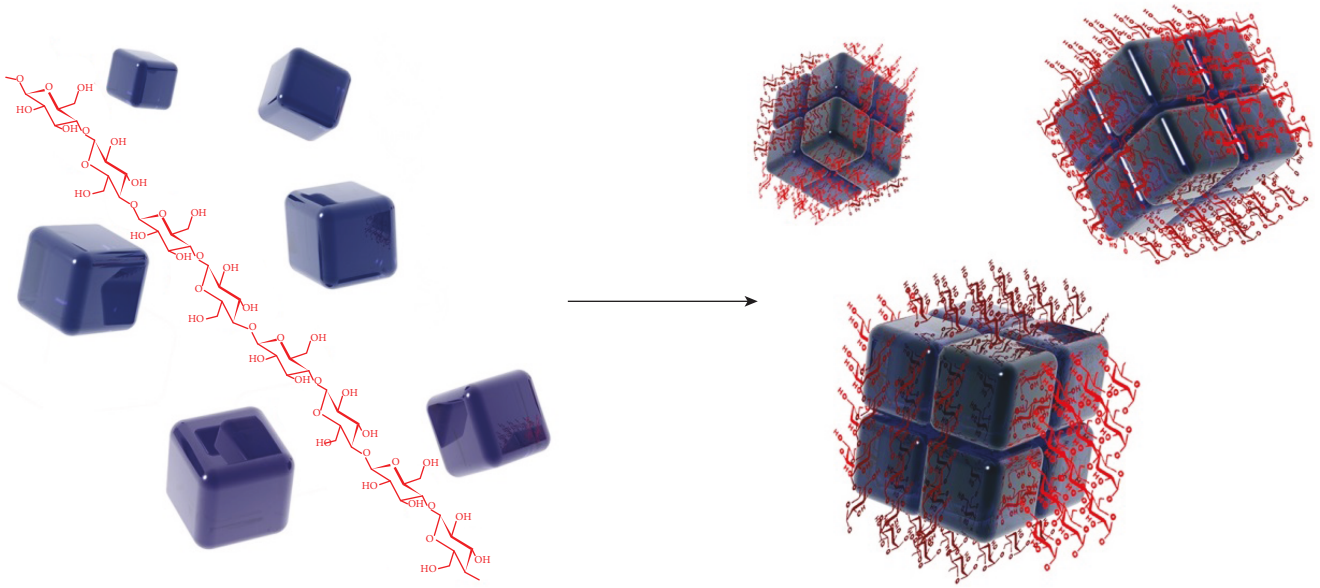

(c)

Figure 2: The sedimentation stability (a) and particle size distribution (b) of dextran-stabilized and nonstabilized WO_3 sols. A possible scheme for doubling the particle size by dextran chains (c).

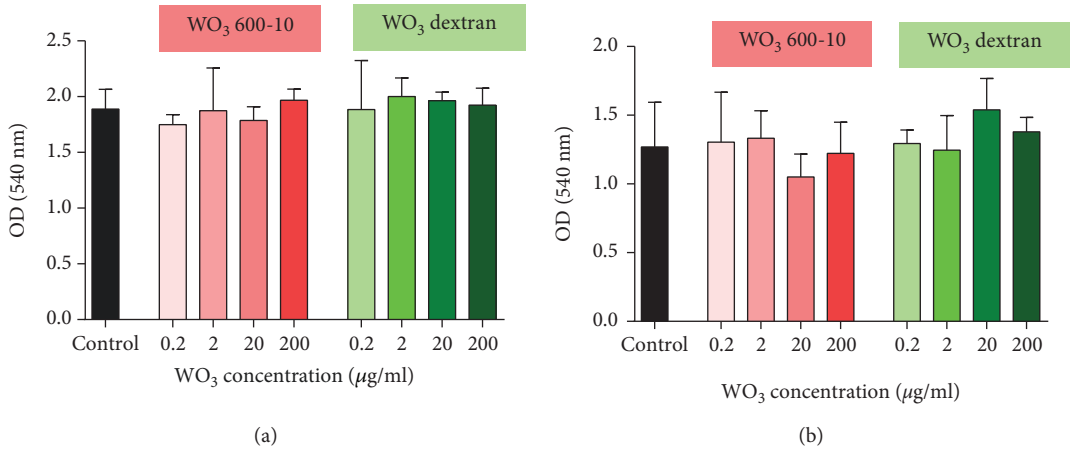

FIGURE 3: MTT assay after 24 hours of incubation with WO_3 nanoparticles. (a) MCF-7 cell line and (b) DPS cells. Data are presented as the mean ± sd (yEr±); $n = 3$. Cells were plated in 96-well plates and left overnight. Then, WO_3 nanoparticles (0.2–200 μg/mL) were added, and after 24 hours, a standard MTT test was performed.

biological media *via* the Haber-Weiss reaction [112]. In this regard, we studied the mitochondrial membrane potential (MMP) after the incubation of the cells with WO_3 nanoparticles (Figure 5). The quantitative analysis of micrographs revealed a slight decrease of MMP in a dose-dependent manner. This decrease suggests that WO_3 nanoparticles still had a certain effect on the cell metabolism, but did not cause cell death, according to the LIVE/DEAD assay.

Next, we performed a morphological analysis of the cell nuclei upon incubation with WO_3 nanoparticles, to detect possible signs of genotoxicity (Figure 6). No visible changes in the nuclear apparatus were observed in either normal or malignant cells in the whole WO_3 nanoparticle concentration range. Nevertheless, a more detailed study should be performed to confirm the absence of genotoxicity (for example, comet assay).

Thus, it can be concluded that WO_3 nanoparticles did not exert short-term (after 24 hours) toxic effects in MCF-7 and DPS cells, although it is worth noting that only the short-term effects of WO_3 nanoparticles on human cells were investigated, while the long-term effects of WO_3 nanoparticle exposure are still to be studied, including long-term cyto-, geno-, and embryotoxicity studies.

4. Discussion

As a rule, tungsten oxide nanoparticles demonstrate low cytotoxicity and are relatively safe *in vitro* in the concentration range of up to 1000 $\mu g\,mL^{-1}$. For example, WO_3 nanoparticles prepared by the electrical arc discharge method in deionized water [113] and coated by cross-linked chitosan demonstrated no significant cytotoxicity at concentrations up to 5000 μg/mL after 24 hours of incubation. Similarly, PEG-poly-ε-caprolactone encapsulated tungsten oxide nanoparticles (average diameter 108 nm, hydrodynamic diameter 152 nm) were synthesized by thermal decomposition of a tungsten precursor (WCl_6) in a polar nonaqueous solvent (diethylene glycol) and modified using a block copolymer [114]. The MTT cytotoxicity assay on HeLa cells demonstrated that obtained nanoparticles exerted a negligible cytotoxic effect within the concentration range of 0.1–5000 μg/mL after 24 h incubation. The same protocol was used for the synthesis of polyacrylic acid-capped tungsten oxide nanoparticles, which also exerted a negligible cytotoxic effect on the A549 human alveolar basal epithelial cell line within the concentration range of 50-1000 μg/mL after 24 hours of incubation [115]. Two-dimensional WO_3 nanoplatelets with sizes ranging from 30 to 100 nm and a thickness of around 5–10 nm were synthesized by thermal decomposition of WCl_6 in a nonpolar solvent, and coated with a poly-ε-caprolactone layer [116]. The cytotoxicity assays on the HeLa cell line demonstrated a LD_{50} value of about 0.01 M (about 2300 $\mu g\,mL^{-1}$) and the absence of toxicity for concentrations up to 0.001 M (about 230 μg/mL). Toxicity profiles of uncoated and coated nanoparticles *in vitro* were very similar, indicating that the polymer did not affect the intrinsic cytotoxicity of WO_3. On the contrary, suspensions of uncoated particles were shown to be extremely toxic *in vivo*, leading to mouse death within a few seconds. Chinde et al. studied the toxicity mechanisms of different concentrations (0–300 μg/mL) of WO_3 nano- and microparticles in human lung carcinoma (A549) cells [117]. The microparticles were nontoxic in the entire range of concentrations studied, while the nanoparticles were nontoxic in the concentration range of up to 100 μg/mL only. The WO_3 concentration of 200 and 300 μg/mL, after 24 h of exposure, led to a significant increase in the percentage of tail DNA, micronucleus formation, and intrinsic apoptotic cell death. Zhou et al. synthesized tungsten oxide nanorods with a length of 13.1 ± 3.6 nm and a diameter of 4.4 ± 1.5 nm by a facile thermal decomposition, then modified them with methoxypoly (ethylene glycol) (PEG) carboxyl acid *via* ligand exchange [118]. According to the MTT cell viability assay (human epithelial cervical cancer cell line HeLa and normal mouse fibroblast cell line L929), these nanoparticles had no cytotoxicity in the dark (without irradiation) in the concentration range up to 125 μg/mL after 4 h incubation. Here, we demonstrated that

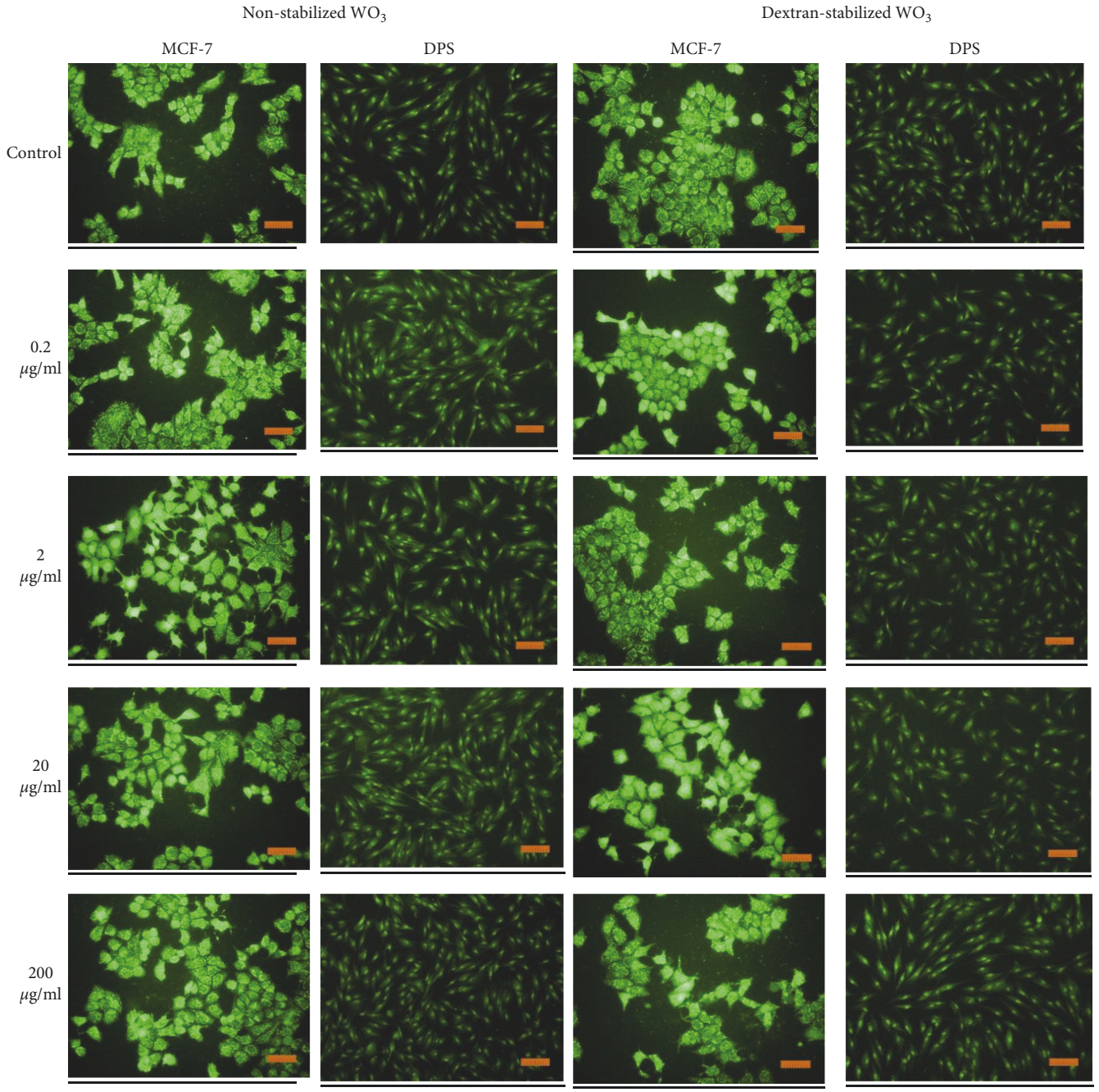

Figure 4: Microphotographs of DPS and MCF-7 cells after 24 hours of incubation with WO_3 nanoparticles (0.2–200 μg/mL). Cells were plated in 96-well plates and left overnight. Then, WO_3 nanoparticles (0.2–200 μg/mL) were added, and after 24 hours, cells were stained with an L-7007 LIVE/DEAD kit.

our novel, facile, and scalable approach to the synthesis of nanocrystalline WO_3 allows for the preparation of stable WO_3 sols containing highly crystalline nanoparticles, which ensures their low cytotoxicity and gives them a prospect for biomedical applications.

Actually, the stability of WO_3 sols is a key prerequisite for their biomedical application, since, generally, due to the high density of tungsten oxide (7.16 g/cm^3), WO_3 nanoparticles precipitate readily. The intermolecular forces of attraction (e.g., those of van der Waals) cause nanoparticle agglomeration/aggregation [119] and sol coagulation/sedimentation [120]. The stability of colloidal solutions depends on the repulsion between nanoparticles; there are two main mechanisms of such repulsion: electrostatic and steric [121, 122]. The former is the result of electrical double layer formation around the nanoparticles due to charge separation. When two nanoparticles approach each other, overlapping their double layers, strong repulsion occurs [123]. This mechanism is dominant in weak electrolytes; the thickness of the double layer drastically decreases at higher ionic

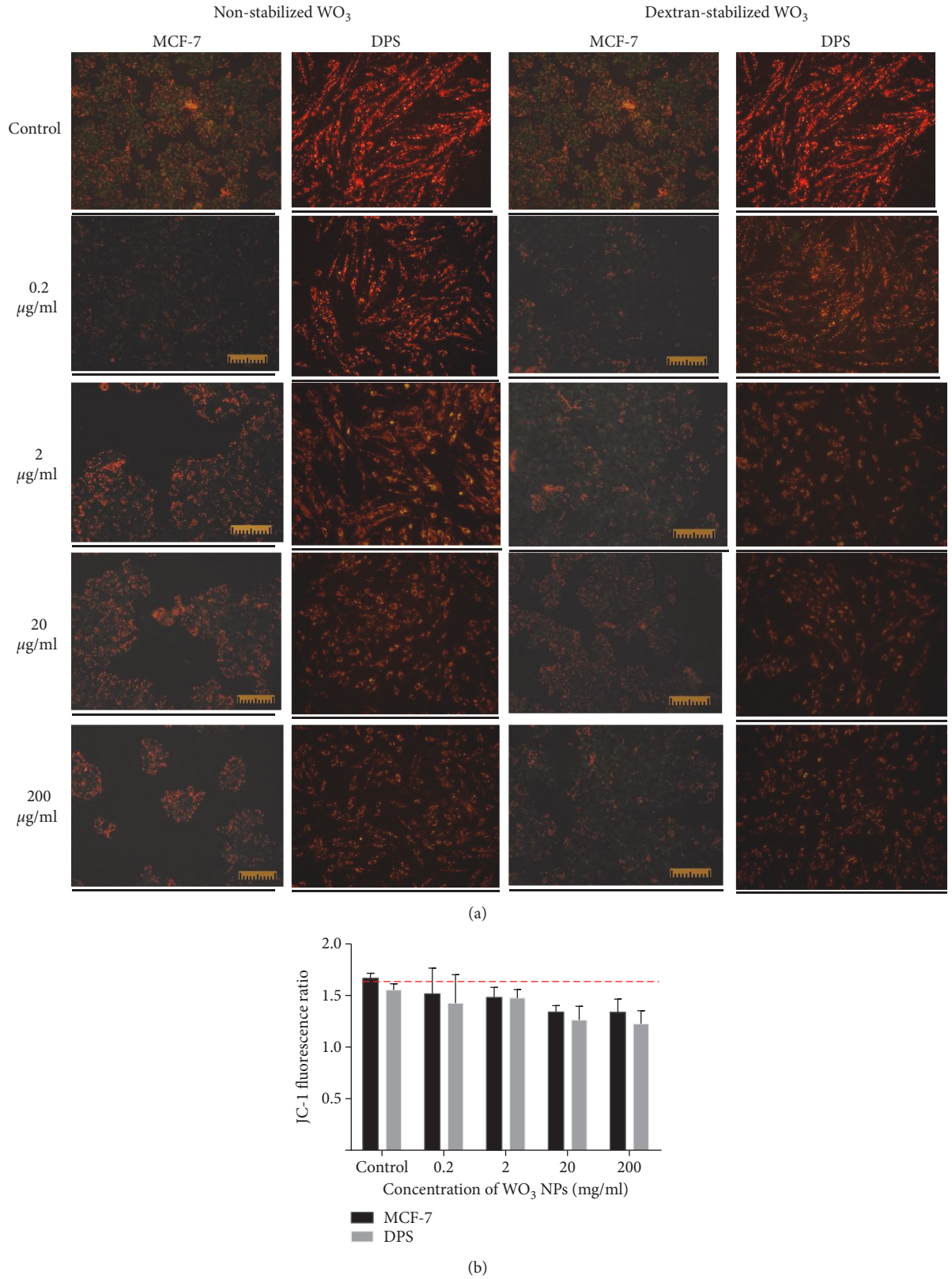

FIGURE 5: The effect of WO_3 NPs on the mitochondrial membrane potential (MMP) in DPS and MCF-7 cells after 24 hours of incubation with WO_3 nanoparticles (0.2–200 μg/mL). Cells were plated in 96-well plates and left overnight. Then, WO_3 nanoparticles (0.2–200 μg/mL) were added, and after 24 hours, cells were stained with JC-1 dye.

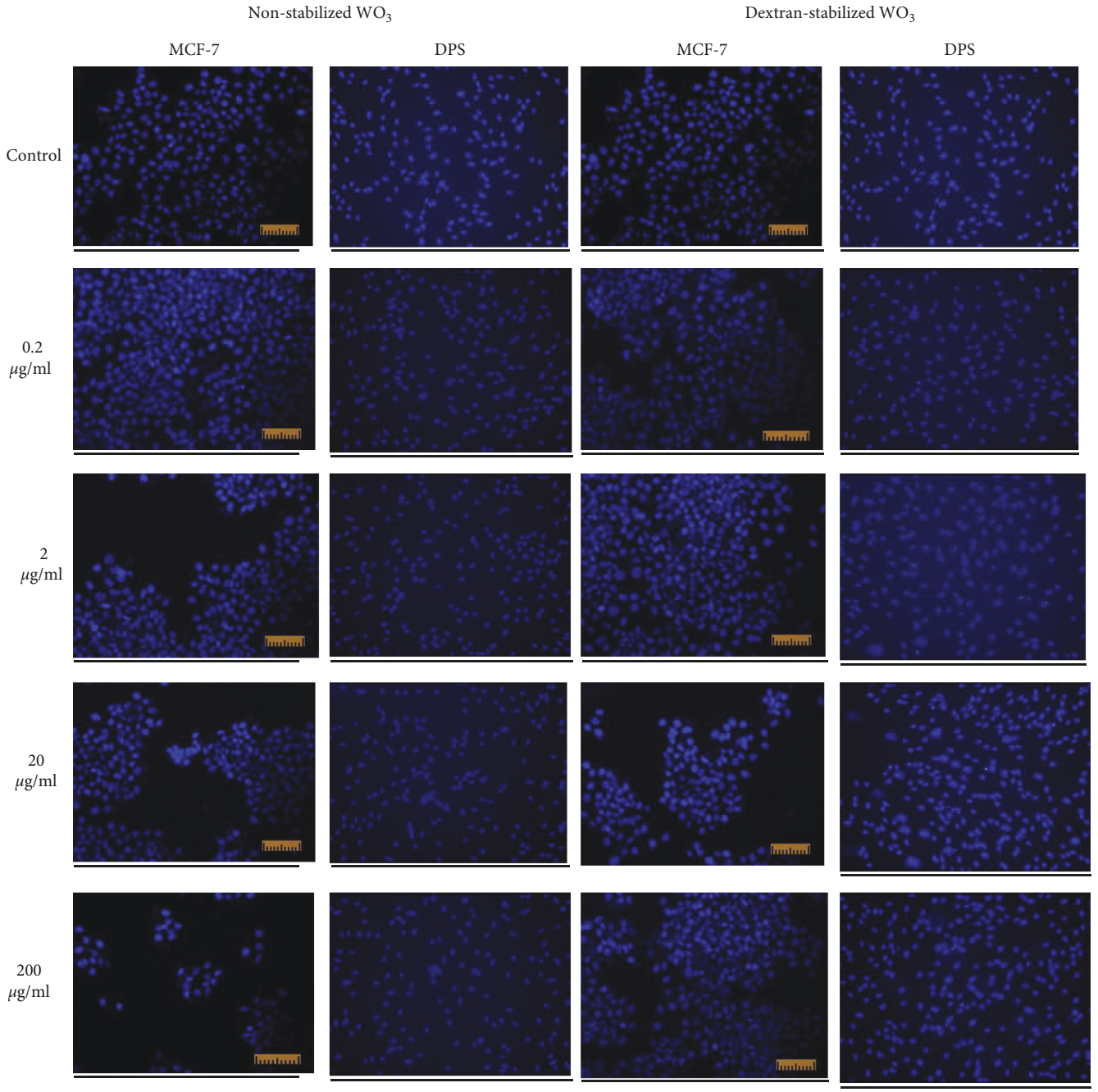

Figure 6: The effect of WO_3 nanoparticles on the nucleic morphology of DPS and MCF-7 cells. Cells were incubated with WO_3 NPs (0.2–200 μg/mL) and, after 24 hours, were stained with Hoechst 33342 dye to detect apoptotic morphology.

concentration, nanoparticles approach much closer, and attraction takes place. Since the biological fluids are strong electrolytes, containing many components, this can cause instability of sols and aggregation of particles [124]. This is why the second, steric mechanism of stabilization should preferably be used for biomedical colloidal system engineering [125, 126]. Here, repulsion is attained by adsorbed big organic molecules (uncharged nonionic surfactants or polymers), forming the protective layer on the surface of nanoparticles, preventing their collision due to the energetically unfavourable interaction of hydrated chains (when the steric stabilizer has good hydrophilicity) [127]. A similar approach was used by Zhou et al. [26] to modify WO_x nanoparticles with methoxypoly (ethylene glycol) carboxyl acid to provide their good water dispersability and biocompatibility.

Generally, in diluted electrolytes, there are no differences in the properties of sols stabilized *via* the two mechanisms, but their behaviour drastically changes in biological media [128–132]. It is a well-known fact that WO_3 nanoparticles having no steric stabilizers (electrostatic stabilization only) are very toxic *in vivo*, probably due to the particles'

aggregation in blood vessels and capillaries [116]. Thus, despite the fact that the stabilizer (dextran) has little effect on the toxicity of tungsten oxide nanoparticles *in vitro*, dextran-stabilized sol is more promising for further *in vivo* applications, for example, in X-ray imaging.

5. Conclusions

Highly crystalline orthorhombic tungsten oxide nanoparticles were synthesized by ammonium paratungstate thermal decomposition, and a very stable aqueous sol was prepared by their ultrasonication. WO_3 nanoparticles were shown to be nontoxic for DPS stem cells and MCF-7 breast cancer cells; they did not cause cell death in the concentration range studied (from 0.2 to 200 μg/mL) and only slightly reduced the metabolic activity of the cells. A nontoxic steric stabilizer (dextran) was proposed for further in vivo administration of WO_3 nanoparticles. The low toxicity of dextran-stabilized WO_3 sol to normal (stem) and malignant cells makes this preparation a possible candidate for biomedical applications including X-ray imaging.

Data Availability

All the data used to support the findings of this study are included within the article and the supplementary information file.

Conflicts of Interest

The authors declare that there is no conflict of interest regarding the publication of this paper.

Acknowledgments

This research has been supported by the Russian Science Foundation (project 18-73-10150).

Supplementary Materials

Table S1: sedimentation stability of stabilized and nonstabilized WO3 sols after 26 days of storage. *(Supplementary Materials)*

References

[1] S. Cong, F. Geng, and Z. Zhao, "Tungsten oxide materials for optoelectronic applications," *Advanced Materials*, vol. 28, no. 47, pp. 10518–10528, 2016.

[2] F. Malara, A. Cannavale, S. Carallo, and G. Gigli, "Smart windows for building integration: a new architecture for photovoltachromic devices," *ACS Applied Materials & Interfaces*, vol. 6, no. 12, pp. 9290–9297, 2014.

[3] C. G. Granqvist, "Electrochromics for smart windows: oxide-based thin films and devices," *Thin Solid Films*, vol. 564, pp. 1–38, 2014.

[4] H. Zheng, Y. Tachibana, and K. Kalantar-Zadeh, "Dye-sensitized solar cells based on WO_3," *Langmuir*, vol. 26, no. 24, pp. 19148–19152, 2010.

[5] A. Marikutsa, L. Yang, M. Rumyantseva, M. Batuk, J. Hadermann, and A. Gaskov, "Sensitivity of nanocrystalline tungsten oxide to CO and ammonia gas determined by surface catalysts," *Sensors and Actuators B: Chemical*, vol. 277, pp. 336–346, 2018.

[6] L. Hu, P. Hu, Y. Chen, Z. Lin, and C. Qiu, "Synthesis and gas-sensing property of highly self-assembled tungsten oxide nanosheets," *Frontiers in Chemistry*, vol. 6, p. 452, 2018.

[7] H. Zhang, W. Chen, and H. Zhang, "Fabrication and characterization of methane gas sensing devices based on 1D tungsten oxide nanostructures," *Journal of Nanoelectronics and Optoelectronics*, vol. 13, no. 8, pp. 1141–1144, 2018.

[8] V. Wood, M. J. Panzer, J. E. Halpert, J. M. Caruge, M. G. Bawendi, and V. Bulović, "Selection of metal oxide charge transport layers for colloidal quantum dot LEDs," *ACS Nano*, vol. 3, no. 11, pp. 3581–3586, 2009.

[9] I. E. Wachs, T. Kim, and E. I. Ross, "Catalysis science of the solid acidity of model supported tungsten oxide catalysts," *Catalysis Today*, vol. 116, no. 2, pp. 162–168, 2006.

[10] C. Di Valentin, F. Wang, and G. Pacchioni, "Tungsten oxide in catalysis and photocatalysis: hints from DFT," *Topics in Catalysis*, vol. 56, no. 15–17, pp. 1404–1419, 2013.

[11] A. Srinivasan and M. Miyauchi, "Chemically stable WO_3 based thin-film for visible-light induced oxidation and superhydrophilicity," *The Journal of Physical Chemistry C*, vol. 116, no. 29, pp. 15421–15426, 2012.

[12] P. Dong, G. Hou, X. Xi, R. Shao, and F. Dong, "WO_3-based photocatalysts: morphology control, activity enhancement and multifunctional applications," *Environmental Science: Nano*, vol. 4, no. 3, pp. 539–557, 2017.

[13] S. Ahmed, I. A. I. Hassan, H. Roy, and F. Marken, "Photoelectrochemical transients for chlorine/hypochlorite formation at "roll-on" nano-WO_3 film electrodes," *The Journal of Physical Chemistry C*, vol. 117, no. 14, pp. 7005–7012, 2013.

[14] M. G. Walter, E. L. Warren, J. R. McKone et al., "Solar water splitting cells," *Chemical Reviews*, vol. 110, no. 11, pp. 6446–6473, 2010.

[15] S. Emin, M. de Respinis, M. Fanetti, W. Smith, M. Valant, and B. Dam, "A simple route for preparation of textured WO_3 thin films from colloidal W nanoparticles and their photoelectrochemical water splitting properties," *Applied Catalysis B: Environmental*, vol. 166-167, pp. 406–412, 2015.

[16] M. R. Waller, T. K. Townsend, J. Zhao et al., "Single-crystal tungsten oxide nanosheets: photochemical water oxidation in the quantum confinement regime," *Chemistry of Materials*, vol. 24, no. 4, pp. 698–704, 2012.

[17] X. Chen, Y. Zhou, Q. Liu, Z. Li, J. Liu, and Z. Zou, "Ultrathin, single-crystal WO_3 nanosheets by two-dimensional oriented attachment toward enhanced photocatalystic reduction of CO_2 into hydrocarbon fuels under visible light," *ACS Applied Materials & Interfaces*, vol. 4, no. 7, pp. 3372–3377, 2012.

[18] P. Wang, B. Huang, X. Qin, X. Zhang, Y. Dai, and M. H. Whangbo, "Ag/AgBr/$WO_3{\cdot}H_2O$: visible-light photocatalyst for bacteria destruction," *Inorganic Chemistry*, vol. 48, no. 22, pp. 10697–10702, 2009.

[19] H. Zheng, J. Z. Ou, M. S. Strano, R. B. Kaner, A. Mitchell, and K. Kalantar-zadeh, "Nanostructured tungsten oxide - properties, synthesis, and applications," *Advanced Functional Materials*, vol. 21, no. 12, pp. 2175–2196, 2011.

[20] N. Soultanidis, W. Zhou, C. J. Kiely, and M. S. Wong, "Solvothermal synthesis of ultrasmall tungsten oxide nanoparticles," *Langmuir*, vol. 28, no. 51, pp. 17771–17777, 2012.

[21] C. Santato, M. Odziemkowski, M. Ulmann, and J. Augustynski, "Crystallographically oriented mesoporous WO_3 films: synthesis, characterization and applications," *Journal of the American Chemical Society*, vol. 123, no. 43, pp. 10639–10649, 2001.

[22] Z. F. Huang, J. Song, L. Pan, X. Zhang, L. Wang, and J. J. Zou, "Tungsten oxides for photocatalysis, electrochemistry, and phototherapy," *Advanced Materials*, vol. 27, no. 36, pp. 5309–5327, 2015.

[23] L. Santos, C. M. Silveira, E. Elangovan et al., "Synthesis of WO_3 nanoparticles for biosensing applications," *Sensors and Actuators B: Chemical*, vol. 223, pp. 186–194, 2016.

[24] A. Staerz, U. Weimar, and N. Barsan, "Understanding the potential of WO_3 based sensors for breath analysis," *Sensors*, vol. 16, no. 11, p. 1815, 2016.

[25] L. Wen, L. Chen, S. Zheng et al., "Ultrasmall biocompatible WO_{3-x} nanodots for multi-modality imaging and combined therapy of cancers," *Advanced Materials*, vol. 28, no. 25, pp. 5072–5079, 2016.

[26] Z. Zhou, B. Kong, C. Yu et al., "Tungsten oxide nanorods: an efficient nanoplatform for tumor CT imaging and photothermal therapy," *Scientific Reports*, vol. 4, no. 1, p. 3653, 2014.

[27] G. R. Bamwenda and H. Arakawa, "The visible light induced photocatalytic activity of tungsten trioxide powders," *Applied Catalysis A: General*, vol. 210, no. 1-2, pp. 181–191, 2001.

[28] A. L. Popov, N. M. Zholobak, O. I. Balko et al., "Photoinduced toxicity of tungsten oxide photochromic nanoparticles," *Journal of Photochemistry and Photobiology B: Biology*, vol. 178, pp. 395–403, 2018.

[29] Z. Chen, Q. Wang, H. Wang et al., "Ultrathin PEGylated $W_{18}O_{49}$ nanowires as a new 980 nm-laser-driven photothermal agent for efficient ablation of cancer cells in vivo," *Advanced Materials*, vol. 25, no. 14, pp. 2095–2100, 2013.

[30] F. Wang, C. Song, W. Guo et al., "Urchin-like tungsten suboxide for photoacoustic imaging-guided photothermal and photodynamic cancer combination therapy," *New Journal of Chemistry*, vol. 41, no. 23, pp. 14179–14187, 2017.

[31] P. Kalluru, R. Vankayala, C.-S. Chiang, and K. C. Hwang, "Photosensitization of singlet oxygen and in vivo photodynamic therapeutic effects mediated by PEGylated $W_{18}O_{49}$ nanowires," *Angewandte Chemie International Edition*, vol. 52, no. 47, pp. 12332–12336, 2013.

[32] J. Qiu, Q. Xiao, X. Zheng et al., "Single $W_{18}O_{49}$ nanowires: a multifunctional nanoplatform for computed tomography imaging and photothermal/photodynamic/radiation synergistic cancer therapy," *Nano Research*, vol. 8, no. 11, pp. 3580–3590, 2015.

[33] https://pubchem.ncbi.nlm.nih.gov/compound/tungsten_trioxide.

[34] S. Adhikari and D. Sarkar, "High efficient electrochromic WO_3 nanofibers," *Electrochimica Acta*, vol. 138, pp. 115–123, 2014.

[35] Q. Q. Sun, M. Xu, S. J. Bao, and C. Ming Li, "pH-controllable synthesis of unique nanostructured tungsten oxide aerogel and its sensitive glucose biosensor," *Nanotechnology*, vol. 26, no. 11, article 115602, 2015.

[36] X. Liu, C. Chen, X.'a. Chen et al., "WO_3 QDs enhanced photocatalytic and electrochemical perfomance of GO/TiO_2 composite," *Catalysis Today*, vol. 315, pp. 155–161, 2018.

[37] S. Cong, Y. Tian, Q. Li, Z. Zhao, and F. Geng, "Single-crystalline tungsten oxide quantum dots for fast pseudocapacitor and electrochromic applications," *Advanced Materials*, vol. 26, no. 25, pp. 4260–4267, 2014.

[38] S. Wang, S. V. Kershaw, G. Li, and M. K. H. Leung, "The self-assembly synthesis of tungsten oxide quantum dots with enhanced optical properties," *Journal of Materials Chemistry C*, vol. 3, no. 14, pp. 3280–3285, 2015.

[39] H. Peng, P. Liu, D. Lin et al., "Fabrication and multifunctional properties of ultrasmall water-soluble tungsten oxide quantum dots," *Chemical Communications*, vol. 52, no. 61, pp. 9534–9537, 2016.

[40] M. Z. Ahmad, A. Z. Sadek, J. Z. Ou, M. H. Yaacob, K. Latham, and W. Wlodarski, "Facile synthesis of nanostructured WO_3 thin films and their characterization for ethanol sensing," *Materials Chemistry and Physics*, vol. 141, no. 2-3, pp. 912–919, 2013.

[41] C. W. Lai, "WO_3 nanoplates film: formation and photocatalytic oxidation studies," *Journal of Nanomaterials*, vol. 2015, Article ID 563587, 7 pages, 2015.

[42] G. Yuan, C. Hua, S. Khan et al., "Improved electrochromic performance of WO_3 films with size controlled nanorods," *Electrochimica Acta*, vol. 260, pp. 274–280, 2018.

[43] Y. Lee, H. J. Choi, T. Kim et al., "Enhanced efficiency of the honeycomb-structured film WO_3 composed of nanorods for electrochromic properties," *Thin Solid Films*, vol. 637, pp. 14–20, 2017.

[44] W.-q. Wang, X.-l. Wang, X.-h. Xia, Z.-j. Yao, Y. Zhong, and J.-p. Tu, "Enhanced electrochromic and energy storage performance in mesoporous WO_3 film and its application in a bi-functional smart window," *Nanoscale*, vol. 10, no. 17, pp. 8162–8169, 2018.

[45] M.-P. Zhuo, F. Liang, Y.-L. Shi et al., "WO_3 nanobelt doped PEDOT:PSS layers for efficient hole-injection in quantum dot light-emitting diodes," *Journal of Materials Chemistry C*, vol. 5, no. 47, pp. 12343–12348, 2017.

[46] B. Moshofsky and T. Mokari, "Length and diameter control of ultrathin nanowires of substoichiometric tungsten oxide with insights into the growth mechanism," *Chemistry of Materials*, vol. 25, no. 8, pp. 1384–1391, 2013.

[47] A. Ghatak, S. Roy Moulik, and B. Ghosh, "Pulsed laser assisted growth of aligned nanowires of WO_3: role of interface with substrate," *RSC Advances*, vol. 6, no. 38, pp. 31705–31716, 2016.

[48] Y. Xiong, Z. Zhu, T. Guo, H. Li, and Q. Xue, "Synthesis of nanowire bundle-like WO_3-$W_{18}O_{49}$ heterostructures for highly sensitive NH_3 sensor application," *Journal of Hazardous Materials*, vol. 353, pp. 290–299, 2018.

[49] X. He, C. Hu, Q. Yi, X. Wang, H. Hua, and X. Li, "Preparation and improved photocatalytic activity of $WO_3 \cdot 0.33H_2O$ nanonetworks," *Catalysis Letters*, vol. 142, no. 5, pp. 637–645, 2012.

[50] Y. Liu, Q. Li, S. Gao, and J. K. Shang, "Template-free solvothermal synthesis of $WO_3/WO_3 \cdot H_2O$ hollow spheres and their enhanced photocatalytic activity from the mixture phase effect," *CrystEngComm*, vol. 16, no. 32, pp. 7493–7501, 2014.

[51] A. B. D. Nandiyanto, O. Arutanti, T. Ogi, F. Iskandar, T. O. Kim, and K. Okuyama, "Synthesis of spherical macroporous WO_3 particles and their high photocatalytic performance," *Chemical Engineering Science*, vol. 101, pp. 523–532, 2013.

[52] S. Adhikari, R. Swain, D. Sarkar, and G. Madras, "Wedge-like WO_3 architectures for efficient electrochromism and photoelectrocatalytic activity towards water pollutants," *Molecular Catalysis*, vol. 432, pp. 76–87, 2017.

[53] J. Zhang, H. Zhang, L. Liu, F. Li, and S. Wang, "$W_{18}O_{49}$ nanorods: controlled preparation, structural refinement, and electric conductivity," *Chemical Physics Letters*, vol. 706, pp. 243–246, 2018.

[54] C.-H. Lu, M. H. Hon, C.-Y. Kuan, and I.-C. Leu, "Preparation of WO_3nanorods by a hydrothermal method for electrochromic device," *Japanese Journal of Applied Physics*, vol. 53, no. 6S, article 06JG08, 2014.

[55] B. Miao, W. Zeng, Y. Mu et al., "Controlled synthesis of monodisperse $WO_3{\cdot}H_2O$ square nanoplates and their gas sensing properties," *Applied Surface Science*, vol. 349, pp. 380–386, 2015.

[56] Q. Chen, J. Li, X. Li et al., "Visible-light responsive photocatalytic fuel cell based on WO_3/W photoanode and Cu_2O/Cu photocathode for simultaneous wastewater treatment and electricity generation," *Environmental Science & Technology*, vol. 46, no. 20, pp. 11451–11458, 2012.

[57] M. Ahmadi and M. J. F. Guinel, "Synthesis and characterization of tungstite (WO3·H2O) nanoleaves and nanoribbons," *Acta Materialia*, vol. 69, pp. 203–209, 2014.

[58] D. H. Kim, "Effects of phase and morphology on the electrochromic performance of tungsten oxide nano-urchins," *Solar Energy Materials and Solar Cells*, vol. 107, pp. 81–86, 2012.

[59] J. Huang, L. Xiao, and X. Yang, "WO_3 nanoplates, hierarchical flower-like assemblies and their photocatalytic properties," *Materials Research Bulletin*, vol. 48, no. 8, pp. 2782–2785, 2013.

[60] M. Xu, W. Zeng, F. Yang, and L. Chen, "Controllability of assemblage from $WO_3{\cdot}H_2O$ nanoplates to nanoflowers with the assistance of oxalic acid," *Journal of Materials Science: Materials in Electronics*, vol. 26, no. 9, pp. 6676–6682, 2015.

[61] H. Kalhori, M. Ranjbar, H. Salamati, and J. M. D. Coey, "Flower-like nanostructures of WO_3: fabrication and characterization of their in-liquid gasochromic effect," *Sensors and Actuators B: Chemical*, vol. 225, pp. 535–543, 2016.

[62] Y. Li, W. A. McMaster, H. Wei, D. Chen, and R. A. Caruso, "Enhanced electrochromic properties of WO_3 nanotree-like structures synthesized via a two-step solvothermal process showing promise for electrochromic window application," *ACS Applied Nano Materials*, vol. 1, no. 6, pp. 2552–2558, 2018.

[63] R. M. Fernández-Domene, R. Sánchez-Tovar, E. Segura-Sanchís, and J. García-Antón, "Novel tree-like WO_3 nanoplatelets with very high surface area synthesized by anodization under controlled hydrodynamic conditions," *Chemical Engineering Journal*, vol. 286, pp. 59–67, 2016.

[64] M. Ullmann, S. K. Friedlander, and A. Schmidt-Ott, "Nanoparticle formation by laser ablation," *Journal of Nanoparticle Research*, vol. 4, no. 6, pp. 499–509, 2002.

[65] Y. Tamou and S. I. Tanaka, "Formation and coalescence of tungsten nanoparticles under electron beam irradiation," *Nanostructured Materials*, vol. 12, no. 1-4, pp. 123–126, 1999.

[66] D. Deniz, D. J. Frankel, and R. J. Lad, "Nanostructured tungsten and tungsten trioxide films prepared by glancing angle deposition," *Thin Solid Films*, vol. 518, no. 15, pp. 4095–4099, 2010.

[67] J. Thangala, S. Vaddiraju, R. Bogale et al., "Large-scale, hot-filament-assisted synthesis of tungsten oxide and related transition metal oxide nanowires," *Small*, vol. 3, no. 5, pp. 890–896, 2007.

[68] C. G. Granqvist, "Electrochromic tungsten oxide films: review of progress 1993–1998," *Solar Energy Materials and Solar Cells*, vol. 60, no. 3, pp. 201–262, 2000.

[69] J. Thangala, S. Vaddiraju, S. Malhotra, V. Chakrapani, and M. K. Sunkara, "A hot-wire chemical vapor deposition (HWCVD) method for metal oxide and their alloy nanowire arrays," *Thin Solid Films*, vol. 517, no. 12, pp. 3600–3605, 2009.

[70] P.-P. R. M. L. Harks, Z. S. Houweling, M. de Jong, Y. Kuang, J. W. Geus, and R. E. I. Schropp, "Metallic tungsten nanostructures and highly nanostructured thin films by deposition of tungsten oxide and subsequent reduction in a single hot-wire CVD process," *Chemical Vapor Deposition*, vol. 18, no. 1-3, pp. 70–75, 2012.

[71] F. Fang, J. Kennedy, J. Futter et al., "Size-controlled synthesis and gas sensing application of tungsten oxide nanostructures produced by arc discharge," *Nanotechnology*, vol. 22, no. 33, article 335702, 2011.

[72] H. K. Kammler, L. Mädler, and S. E. Pratsinis, "Flame synthesis of nanoparticles," *Chemical Engineering & Technology*, vol. 24, no. 6, pp. 583–596, 2001.

[73] C. P. Li, C. A. Wolden, A. C. Dillon, and R. C. Tenent, "Electrochromic films produced by ultrasonic spray deposition of tungsten oxide nanoparticles," *Solar Energy Materials and Solar Cells*, vol. 99, pp. 50–55, 2012.

[74] O. Arutanti, T. Ogi, A. B. D. Nandiyanto, F. Iskandar, and K. Okuyama, "Controllable crystallite and particle sizes of WO_3 particles prepared by a spray-pyrolysis method and their photocatalytic activity," *AICHE Journal*, vol. 60, no. 1, pp. 41–49, 2014.

[75] S. Supothina, P. Seeharaj, S. Yoriya, and M. Sriyudthsak, "Synthesis of tungsten oxide nanoparticles by acid precipitation method," *Ceramics International*, vol. 33, no. 6, pp. 931–936, 2007.

[76] H. F. Pang, X. Xiang, Z. J. Li, Y. Q. Fu, and X. T. Zu, "Hydrothermal synthesis and optical properties of hexagonal tungsten oxide nanocrystals assisted by ammonium tartrate," *Physica Status Solidi (A)*, vol. 209, no. 3, pp. 537–544, 2012.

[77] N. Huo, S. Yang, Z. Wei, and J. Li, "Synthesis of WO_3 nanostructures and their ultraviolet photoresponse properties," *Journal of Materials Chemistry C*, vol. 1, no. 25, pp. 3999–4007, 2013.

[78] C. J. Hung, Y. H. Huang, C. H. Chen, P. Lin, and T. Y. Tseng, "Hydrothermal formation of tungsten trioxide nanowire networks on seed-free substrates and their properties in electrochromic device," *IEEE Transactions on Components, Packaging and Manufacturing Technology*, vol. 4, no. 5, pp. 831–839, 2014.

[79] K. Lee, W. S. Seo, and J. T. Park, "Synthesis and optical properties of colloidal tungsten oxide nanorods," *Journal of the American Chemical Society*, vol. 125, no. 12, pp. 3408-3409, 2003.

[80] H. G. Choi, Y. H. Jung, and D. K. Kim, "Solvothermal synthesis of tungsten oxide nanorod/nanowire/nanosheet," *Journal of the American Ceramic Society*, vol. 88, no. 6, pp. 1684–1686, 2005.

[81] M. Breedon, P. Spizzirri, M. Taylor et al., "Synthesis of nanostructured tungsten oxide thin films: a simple, controllable, inexpensive, aqueous sol–gel method," *Crystal Growth & Design*, vol. 10, no. 1, pp. 430–439, 2010.

[82] C. Costa, C. Pinheiro, I. Henriques, and C. A. T. Laia, "Inkjet printing of sol–gel synthesized hydrated tungsten oxide nanoparticles for flexible electrochromic devices," *ACS Applied Materials & Interfaces*, vol. 4, no. 3, pp. 1330–1340, 2012.

[83] M. Niederberger, "Nonaqueous sol–gel routes to metal oxide nanoparticles," *Accounts of Chemical Research*, vol. 40, no. 9, pp. 793–800, 2007.

[84] M. Boutonnet, S. Lögdberg, and E. Elm Svensson, "Recent developments in the application of nanoparticles prepared from w/o microemulsions in heterogeneous catalysis," *Current Opinion in Colloid & Interface Science*, vol. 13, no. 4, pp. 270–286, 2008.

[85] S. N. Khadzhiev, K. M. Kadiev, G. P. Yampolskaya, and M. K. Kadieva, "Trends in the synthesis of metal oxide nanoparticles through reverse microemulsions in hydrocarbon media," *Advances in Colloid and Interface Science*, vol. 197-198, pp. 132–145, 2013.

[86] L. Xiong and T. He, "Synthesis and characterization of ultrafine tungsten and tungsten oxide nanoparticles by a reverse microemulsion-mediated method," *Chemistry of Materials*, vol. 18, no. 9, pp. 2211–2218, 2006.

[87] R. Abazari, A. R. Mahjoub, L. A. Saghatforoush, and S. Sanati, "Characterization and optical properties of spherical WO_3 nanoparticles synthesized via the reverse microemulsion process and their photocatalytic behavior," *Materials Letters*, vol. 133, pp. 208–211, 2014.

[88] M. Deepa, M. Kar, D. P. Singh, A. K. Srivastava, and S. Ahmad, "Influence of polyethylene glycol template on microstructure and electrochromic properties of tungsten oxide," *Solar Energy Materials and Solar Cells*, vol. 92, no. 2, pp. 170–178, 2008.

[89] K. Zhu, H. He, S. Xie et al., "Crystalline WO_3 nanowires synthesized by templating method," *Chemical Physics Letters*, vol. 377, no. 3-4, pp. 317–321, 2003.

[90] S. H. Baeck, T. Jaramillo, G. D. Stucky, and E. W. McFarland, "Controlled electrodeposition of nanoparticulate tungsten oxide," *Nano Letters*, vol. 2, no. 8, pp. 831–834, 2002.

[91] C. J. Chen and D. H. Chen, "Preparation and near-infrared photothermal conversion property of cesium tungsten oxide nanoparticles," *Nanoscale Research Letters*, vol. 8, no. 1, p. 57, 2013.

[92] H. Yan, X. Zhang, S. Zhou, X. Xie, Y. Luo, and Y. Yu, "Synthesis of WO_3 nanoparticles for photocatalytic O_2 evolution by thermal decomposition of ammonium tungstate loading on g-C_3N_4," *Journal of Alloys and Compounds*, vol. 509, no. 24, pp. L232–L235, 2011.

[93] M. J. G. Fait, H. J. Lunk, M. Feist, M. Schneider, J. N. Dann, and T. A. Frisk, "Thermal decomposition of ammonium paratungstate tetrahydrate under non-reducing conditions: characterization by thermal analysis, X-ray diffraction and spectroscopic methods," *Thermochimica Acta*, vol. 469, no. 1-2, pp. 12–22, 2008.

[94] M. S. Marashi, J. Vahdati Khaki, and S. M. Zebarjad, "Comparing thermal and mechanochemical decomposition of ammonium paratungstate (APT)," *International Journal of Refractory Metals and Hard Materials*, vol. 30, no. 1, pp. 177–179, 2012.

[95] M. J. G. Fait and H.-J. Lunk, "Thermal decomposition of ammonium paratungstate tetrahydrate traced by in situ UV/Vis diffuse reflectance spectroscopy," *European Journal of Inorganic Chemistry*, vol. 2012, no. 2, pp. 213–216, 2012.

[96] A. O. Kalpakli, A. Arabaci, C. Kahruman, and I. Yusufoglu, "Thermal decomposition of ammonium paratungstate hydrate in air and inert gas atmospheres," *International Journal of Refractory Metals and Hard Materials*, vol. 37, pp. 106–116, 2013.

[97] A. Eser, C. Kahruman, and I. Yusufoglu, "Thermal decomposition reaction mechanisms and kinetics of ammonium paratungstate tetrahydrate," in *Characterization of Minerals, Metals, and Materials*, pp. 645–654, John Wiley & Sons, Inc., 2014.

[98] D. Hunyadi, I. Sajó, and I. M. Szilágyi, "Structure and thermal decomposition of ammonium metatungstate," *Journal of Thermal Analysis and Calorimetry*, vol. 116, no. 1, pp. 329–337, 2014.

[99] M. J. G. Fait, E. Moukhina, M. Feist, and H. J. Lunk, "Thermal decomposition of ammonium paratungstate tetrahydrate: new insights by a combined thermal and kinetic analysis," *Thermochimica Acta*, vol. 637, pp. 38–50, 2016.

[100] F. Pan, Q. Zhu, S. Li, M. Xiang, and Z. Du, "Decomposition-carbonization of ammonium paratungstate in a fluidized bed," *International Journal of Refractory Metals and Hard Materials*, vol. 72, pp. 315–322, 2018.

[101] V. Singh and I. B. Sharma, "Study of thermal decomposition of ammonium paratungstate," *Materials Today: Proceedings*, vol. 5, no. 7, pp. 15277–15284, 2018.

[102] T. O. Shekunova, A. E. Baranchikov, A. D. Yapryntsev et al., "Ultrasonic disintegration of tungsten trioxide pseudomorphs after ammonium paratungstate as a route for stable aqueous sols of nanocrystalline WO_3," *Journal of Materials Science*, vol. 53, no. 3, pp. 1758–1768, 2018.

[103] A. B. D. Nandiyanto, R. Zaen, and R. Oktiani, "Correlation between crystallite size and photocatalytic performance of micrometer-sized monoclinic WO_3 particles," *Arabian Journal of Chemistry*, 2017, https://www.sciencedirect.com/science/article/pii/S1878535217302046.

[104] S. Chinde and P. Grover, "Toxicological assessment of nano and micron-sized tungsten oxide after 28 days repeated oral administration to Wistar rats," *Mutation Research/Genetic Toxicology and Environmental Mutagenesis*, vol. 819, pp. 1–13, 2017.

[105] A. Pessina, A. Bonomi, V. Coccè et al., "Mesenchymal stromal cells primed with paclitaxel provide a new approach for cancer therapy," *PLoS One*, vol. 6, no. 12, article e28321, 2011.

[106] D. Gjorgieva Ackova, T. Kanjevac, L. Rimondini, and D. Bosnakovski, "Perspectives in engineered mesenchymal stem/stromal cells based anti- cancer drug delivery systems," *Recent Patents on Anti-Cancer Drug Discovery*, vol. 11, no. 1, pp. 98–111, 2016.

[107] E. Ledesma-Martínez, V. M. Mendoza-Núñez, and E. Santiago-Osorio, "Mesenchymal stem cells derived from dental pulp: a review," *Stem Cells International*, vol. 2016, Article ID 4709572, 12 pages, 2016.

[108] L. G. Menon, J. Pratt, H. W. Yang, P. M. Black, G. A. Sorensen, and R. S. Carroll, "Imaging of human mesenchymal stromal cells: homing to human brain tumors," *Journal of Neuro-Oncology*, vol. 107, no. 2, pp. 257–267, 2012.

[109] E. Synowiec, G. Hoser, K. Wojcik, E. Pawlowska, T. Skorski, and J. Błasiak, "UV differentially induces oxidative stress, DNA damage and apoptosis in BCR-ABL1-positive cells sensitive and resistant to imatinib," *International Journal of Molecular Sciences*, vol. 16, no. 8, pp. 18111–18128, 2015.

[110] A. B. Djurišić, Y. H. Leung, A. M. C. Ng et al., "Toxicity of metal oxide nanoparticles: mechanisms, characterization and avoiding experimental artefacts," *Small*, vol. 11, no. 1, pp. 26–44, 2015.

[111] A. Manke, L. Wang, and Y. Rojanasakul, "Mechanisms of nanoparticle-induced oxidative stress and toxicity," *BioMed Research International*, vol. 2013, Article ID 942916, 15 pages, 2013.

[112] M. Yang, X. Zhang, A. Grosjean, I. Soroka, and M. Jonsson, "Kinetics and mechanism of the reaction between H_2O_2 and tungsten powder in water," *The Journal of Physical Chemistry C*, vol. 119, no. 39, pp. 22560–22569, 2015.

[113] M. Firouzi, R. Poursalehi, H. Delavari H, F. Saba, and M. A. Oghabian, "Chitosan coated tungsten trioxide nanoparticles as a contrast agent for X-ray computed tomography," *International Journal of Biological Macromolecules*, vol. 98, pp. 479–485, 2017.

[114] J. Mu, X. Meng, L. Chen et al., "Highly stable and biocompatible $W_{18}O_{49}$@PEG-PCL hybrid nanospheres combining CT imaging and cancer photothermal therapy," *RSC Advances*, vol. 7, no. 18, pp. 10692–10699, 2017.

[115] D. Huo, J. He, H. Li et al., "X-ray CT guided fault-free photothermal ablation of metastatic lymph nodes with ultrafine HER-2 targeting $W_{18}O_{49}$ nanoparticles," *Biomaterials*, vol. 35, no. 33, pp. 9155–9166, 2014.

[116] A. Jakhmola, N. Anton, H. Anton et al., "Poly-ε-caprolactone tungsten oxide nanoparticles as a contrast agent for X-ray computed tomography," *Biomaterials*, vol. 35, no. 9, pp. 2981–2986, 2014.

[117] S. Chinde, Y. Poornachandra, A. Panyala et al., "Comparative study of cyto- and genotoxic potential with mechanistic insights of tungsten oxide nano- and microparticles in lung carcinoma cells," *Journal of Applied Toxicology*, vol. 38, no. 6, pp. 896–913, 2018.

[118] H. Zhou, Y. Shi, Q. Dong et al., "Interlaced $W_{18}O_{49}$ nanofibers as a superior catalyst for the counter electrode of highly efficient dye-sensitized solar cells," *Journal of Materials Chemistry A*, vol. 2, no. 12, pp. 4347–4354, 2014.

[119] S. V. Sokolov, K. Tschulik, C. Batchelor-McAuley, K. Jurkschat, and R. G. Compton, "Reversible or not? Distinguishing agglomeration and aggregation at the nanoscale," *Analytical Chemistry*, vol. 87, no. 19, pp. 10033–10039, 2015.

[120] A. Ghadimi, R. Saidur, and H. S. C. Metselaar, "A review of nanofluid stability properties and characterization in stationary conditions," *International Journal of Heat and Mass Transfer*, vol. 54, no. 17-18, pp. 4051–4068, 2011.

[121] T. Tadros, "Electrostatic and steric stabilization of colloidal dispersions," in *Electrical Phenomena at Interfaces and Biointerfaces: Fundamentals and Applications in Nano-, Bio- and Environmental Sciences*, p. 153, John Wiley & Sons, Inc., 2012.

[122] I. D. Morrison and S. Ross, *Colloidal Dispersions: Suspensions, Emulsions, and Foams*, Wiley-Interscience, New York, NY, USA, 2002.

[123] M. A. Brown, Z. Abbas, A. Kleibert et al., "Determination of surface potential and electrical double-layer structure at the aqueous electrolyte-nanoparticle interface," *Physical Review X*, vol. 6, no. 1, 2016.

[124] W. Norde, *Colloids and Interfaces in Life Sciences*, Marcel Dekker, New York, NY, USA, 2003.

[125] H. Ohshima, Ed., *Electrical Phenomena at Interfaces and Biointerfaces: Fundamentals and Applications in Nano-, Bio- and Environmental Sciences*, John Wiley & Sons, Inc., 2012.

[126] H. Otsuka, Y. Nagasaki, and K. Kataoka, "PEGylated nanoparticles for biological and pharmaceutical applications," *Advanced Drug Delivery Reviews*, vol. 64, pp. 246–255, 2012.

[127] A. Vrij, "Polymers at interfaces and the interactions in colloidal dispersions," *Pure and Applied Chemistry*, vol. 48, no. 4, pp. 471–483, 1976.

[128] R. Fåhraeus, "The suspension stability of the blood," *Physiological Reviews*, vol. 9, no. 2, pp. 241–274, 1929.

[129] J. Jiang, G. Oberdörster, and P. Biswas, "Characterization of size, surface charge, and agglomeration state of nanoparticle dispersions for toxicological studies," *Journal of Nanoparticle Research*, vol. 11, no. 1, pp. 77–89, 2009.

[130] F. W. Tavares, D. Bratko, H. W. Blanch, and J. M. Prausnitz, "Ion-specific effects in the colloid–colloid or protein–protein potential of mean force: role of salt–macroion van der Waals interactions," *The Journal of Physical Chemistry B*, vol. 108, no. 26, pp. 9228–9235, 2004.

[131] L. Treuel, K. A. Eslahian, D. Docter et al., "Physicochemical characterization of nanoparticles and their behavior in the biological environment," *Physical Chemistry Chemical Physics*, vol. 16, no. 29, pp. 15053–15067, 2014.

[132] S. Bhattacharjee, "DLS and zeta potential – what they are and what they are not?," *Journal of Controlled Release*, vol. 235, pp. 337–351, 2016.